Journal of Alloys and Compounds 873 (2021) 159784

Contents lists available at ScienceDirect

Journal of Alloys and Compounds

journal homepage: www.elsevier.com/locate/jalcom

Influence of heterovalent cationic substitution on electrical properties of $Ag_{6+x}(P_{1-x}Ge_x)S_5I$ solid solutions

I.P. Studenyak[a,*], A.I. Pogodin[a], M.J. Filep[a,b], O.I. Symkanych[a], T.Y. Babuka[a], O.P. Kokhan[a], P. Kúš[c]

[a] Uzhhorod National University, Pidgirna Street 46, Uzhhorod 88000, Ukraine
[b] Ferenc Rákóczi II Transcarpathian Hungarian Institute, Kossuth Sq. 6, Beregovo 90200, Ukraine
[c] Comenius University, Mlynska dolina, Bratislava 84248, Slovakia

ARTICLE INFO

Article history:
Received 5 March 2021
Accepted 1 April 2021
Available online 8 April 2021

Keywords:
Argyrodites
Superionic conductors
Single crystals
Solid solutions
Electrical conductivity
Crystal structure

ABSTRACT

High-quality single crystals of $Ag_{6+x}(P_{1-x}Ge_x)S_5I$ (0.25, 0.5, 0.75) solid solutions are grown from the solution–melt by vertical zone crystallization method. In order to study the crystal structure and to establish the mechanism of formation of $Ag_{6+x}(P_{1-x}Ge_x)S_5I$ solid solutions as well as to explain the peculiarities of ion transport, the investigation of the single crystals was carried out using XRD analysis by the Rietveld method based on the refined models of initial Ag_6PS_5I and Ag_7GeS_5I structures. The measurements of electrical conductivity of single-crystal $Ag_{6+x}(P_{1-x}Ge_x)S_5I$ samples was performed using impedance spectroscopy method in frequency range of 1×10^1–2×10^6 Hz and temperature interval of 293–383 K. Ionic and electronic components of electrical conductivity are determined using Nyquist plots. Based on the analysis of compositional dependences, it was found that for solid solutions the maximum of the ionic component of electrical conductivity and the minimum of its activation energy are observed. The features of the ion transport mechanism in $Ag_{6+x}(P_{1-x}Ge_x)S_5I$ solid solutions with a heterovalent substitution are explained.

1. Introduction

Argyrodites as a wide class of tetrahedrally densely packed ternary and quaternary compounds got its name from the mineral Ag_8GeS_6 [1]. At present, a significant number of argyrodite structure representatives [1–3] are known, the general formula of which is given in Ref. [2]. The argyrodite structure always includes two types of cations: single-charge (type A) and multi-charge (type B). Cations of type B, with valence from 3 to 5, are tetrahedrally coordinated by anions and form a rigid anionic frame, as well as the single-charged (rarely two-charge) type A cations are in the voids between them and have different crystallographic positions [1,2].

The most studied are ternary and quaternary argyrodites, which include multi-charge (Si^{4+}, Ge^{4+}, P^{5+}) and single charge (Cu^+, Ag^+, Li^+) cations [3–9]. It should be noted that single- and multi-charge cations are subject to isomorphic substitution, resulting in a large number of existing solid solutions [10–14]. Argyrodite structure compounds have interesting physical properties and can be successfully used as optical, ferroelastic, thermoelectric materials [7–11,14–18]. However, due to the peculiarities of their crystal structure providing high ionic conductivity due to the disordered sublattice of type A cations, the greatest number of investigations is devoted to compounds of argyrodite structure as promising solid-electrolytic materials.

To improve the physico-chemical parameters of the aforementioned materials, studies of both isovalent and heterovalent substitution of atoms are actively performed [19–24]. Thus, in Refs. [21–24] the possibility of increasing ionic conductivity and reducing activation energy by $P^{5+}\leftrightarrow Ge^{4+}$ ($Li_{6+x}P_{1-x}Ge_xS_5I$) та $P^{5+}\leftrightarrow Si^{4+}$ ($Li_{6+x}P_{1-x}Si_xS_5Br$) heterovalent substitutions is shown.

Ag^+-containing materials have high values of electrical conductivity. Thus, for Ag_6PS_5I the value of the total electrical conductivity is 1.2×10^{-4} S/cm (300 K) [7]. For Ag_7GeS_5I the value of the total electrical conductivity is 4.7×10^{-2} S/cm [20], while the value of the ionic component of electrical conductivity is 7.98×10^{-3} S/cm (298 K) [19]. The proximity of values of Ag_6PS_5I and Ag_7GeS_5I lattice parameters [7,25] indicates the possibility of the formation of solid solutions based on them. That is why it was decided to study the $P^{5+}\leftrightarrow Ge^{4+}$ heterovalent substitution within Ag_6PS_5I–Ag_7GeS_5I system.

In this respect, the aim of this paper is to grow $Ag_{6+x}(P_{1-x}Ge_x)S_5I$ (0.25, 0.5, 0.75) single crystals, study the interrelation between

* Corresponding author.
E-mail address: studenyak@dr.com (I.P. Studenyak).

https://doi.org/10.1016/j.jallcom.2021.159784
0925-8388/

structure and electrical properties, investigate the compositional behavior of electrical conductivity, compositional disordering processes and ion transport mechanism.

2. Experimental

Alloys of Ag_6PS_5I – Ag_7GeS_5I system were synthesized by direct one-temperature method from pre-synthesized tetrahedral Ag_6PS_5I and Ag_7GeS_5I. Synthesis of Ag_6PS_5I and Ag_7GeS_5I was carried out from simple substances: silver (99.995%), phosphorus (99.99%), sulfur (99.999%), germanium (99.99%) and presynthesized binary argentum (I) iodide, additionally purified by directional crystallization method, taken in stoichiometric ratios in vacuumed up to 0.13 Pa quartz ampoules. Synthesis mode for Ag_6PS_5I and Ag_7GeS_5I included a stepped heating up to 723 K at a rate of 100 K/h (exposure during 48 h), a further increase in temperature to 1100 K for Ag_6PS_5I and 1273 K for Ag_7GeS_5I at 50 K/h and exposure at this temperature for 24 h. Synthesis mode of alloys within Ag_6PS_5I – Ag_7GeS_5I system included stepped heating at a rate of 100 K/h to 1273 K and exposure during 72 h. The annealing temperature was 733 K (120 h shuttering). Cooling to room temperature was carried out in the oven off mode.

Growing of $Ag_{6+x}(P_{1-x}Ge_x)S_5I$ (0.25, 0.5, 0.75) crystals was carried out by crystallization from solution-melt in a two-zone tubular resistance furnace using a quartz container of special configuration. Technological conditions for growing $Ag_{6+x}(P_{1-x}Ge_x)S_5I$ crystals are given in Table 1. In order to homogenize the melt, 24 h of ampoule exposure was carried out at temperatures in the range 1143–1203 K (~50 K more than T_m) in the melt zone (Table 1). The process of the crystal growing consists of the formation of the embryo in the lower conical portion of the container by the method of recrystallization in the course of 24 h and the crystal build-up on the formed seed. The optimum rate of crystallization front movement was 0.4–0.5 mm/h, annealing temperature determined as ~2/3 T_m was in the range 730–770 K (72 h), cooling to room temperature at a rate −5 K/h. By this method, the crystals of $Ag_{6+x}(P_{1-x}Ge_x)S_5I$ solid solutions of dark gray color with a metallic luster, 30–40 mm in length and 10–12 mm in diameter were obtained.

In order to study the crystal structure peculiarities of $Ag_{6+x}(P_{1-x}Ge_x)S_5I$ ($x = 0.25, 0.5, 0.75$) solid solutions caused by $P^{+5} \leftrightarrow Ge^{+4}$ heterovalent cationic substitution, and to determine their effect on ionic conductivity, the study of the obtained single crystals was carried out by the Rietveld XRD analysis [26,27]. Determining basic structural parameters was carried out on the basis of refined models of initial structures of Ag_6PS_5I and Ag_7GeS_5I [25]. Experimental data (Fig. 1) were obtained using the AXRD Benchtop (Proto Manufacturing Limited) diffractometer (hybrid photon counting detector) DECTRIS MYTHEN2R 1D, shooting geometry – Bragg-Brentano θ/2θ, CUKα radiation (Ni - filter), angle scanning range −10–120° 2° θ with dynamic ROI (dynamic region of interest), exposition 1 s. Calculation and refinement of the model was carried out using the program EXPO 2014 [28,29], visualization – using VESTA 3.4.4 [30].

Investigations of electrical conductivity of $Ag_{6+x}(P_{1-x}Ge_x)S_5I$ ($x = 0.25, 0.5, 0.75$) solid solutions performed out by impedance spectroscopy [31] in frequency range (1×10^1–2×10^6 Hz) and temperature interval (293–383 K) using high-precision LCR meters Keysight E4980A and AT 2818. The amplitude of the alternating current constituted 10 mV. Measurements were carried out by a two-electrode method on blocking (electronic) gold contacts, which were applied by chemical precipitation from solutions. The analysis of the received dependencies using the Nyquist plots was carried out in the program ZView 3.5.

3. Results and discussion

3.1. Crystal structure

Ag_6PS_5I and Ag_7GeS_5I compounds crystallize in a face-centered cubic cell of argyrodite structure [1,2], SG (spatial group F-43 m, Z=4) with lattice parameters a= 10.4745 (1) for Ag_6PS_5I and a= 10.6832 (4) for Ag_7GeS_5I, respectively, which are well consistent with the literature data [7,13,19,20,25]. Based on the results of the full-profile analysis by the Rietveld method (Fig. 1), it is established that a continuous series of $Ag_{6+x}(P_{1-x}Ge_x)S_5I$ solid solutions is formed in Ag_6PS_5I – Ag_7GeS_5I system. The latter is also confirmed by the compositional dependence of the lattice parameter, which is shown on the insert in Fig. 1. Thus, the investigated $Ag_{6+x}(P_{1-x}Ge_x)S_5I$ ($x = 0.25, 0.5, 0.75$) solid solutions crystallize in the structure of argyrodite SG (spatial group F-43 m, Z = 4). The change of the cubic lattice parameter (insert to Fig. 1) occurs with insignificant positive deviations from the Vegard law, which indicates the compositional disordering of the crystal structure in the formation of a solid solution.

Let us consider in more detail the mechanism of heterovalent $P^{+5} \rightarrow Ge^{+4}$ cationic substitution within an anionic sublattice for $Ag_{6+x}(P_{1-x}Ge_x)S_5I$ ($x = 0.25, 0.5, 0.75$) solid solutions on the example of coordination polyhedra. The basis of the anionic framework of Ag_6PS_5I and Ag_7GeS_5I compounds consists of $[P(Ge)S_4]$, $[S_3I]$ and $[SI_4]$ tetrahedra, of which icosahedra are formed, and that is characteristic for all compounds with the argyrodite structure [2]. In the process of solid solutions formation phosphorus substitution on germanium occurs in position P1 (4b), which causes the formation of common position P1Ge1. As a result, the structure of $Ag_{6+x}(P_{1-x}Ge_x)S_5I$ ($x = 0.25, 0.5, 0.75$) anionic sublattice appears to have $[(PGe)S_4]$ tetrahedra in its basis (Fig. 2a). Icosahedra (Fig. 2b) formed from $[(PGe)S_4]$, $[S_3I]$ and $[SI_4]$ tetrahedra, are coordinated around the sulfur atom S1 (16e), which is simultaneously the vertex of the tetrahedra $[(PGe)S_4]$. Since the structure of argyrodite is characterized by the presence of interpenetrating icosahedra, the sulfur atom S1 (16e) is also the vertex of the next $[SS_9I_3]$ icosahedron.

Obviously, the heterovalent substitution $P^{+5} \rightarrow Ge^{+4}$ causes the disordering of the anionic sublattice of crystalline structures of $Ag_{6+x}(P_{1-x}Ge_x)S_5I$ ($x = 0.25, 0.5, 0.75$) solid solutions. This leads to the disordering of the mobile cationic sublattice, which is due to the presence of doubled $[AgS_3I_2]$ tetrahedra, the last are components of icosahedra (Fig. 2b). The doubled tetrahedra are coordinated around Ag1 and Ag2 positions (Fig. 3) by S1, S2 sulfur atoms and I1 iodine atom.

Thus, in the structure of $Ag_{6+x}(P_{1-x}Ge_x)S_5I$ ($x = 0.25, 0.5, 0.75$) solid solutions, two symmetrically independent silver atoms can be distinguished in the positions Ag1 (24 g) and Ag2 (48 h), with Ag1 atom being in triangular coordination of sulfur atoms (S1S2S1) with a slight displacement to the S1S2 edge, while the Ag2 atom is tetrahedrally coordinated (S1S2S1I1) with displacement to the planes of triangles (S1S2S1) and (S1S2I1) (Fig. 3).

Table 1
Technological conditions for growing of $Ag_{6+x}(P_{1-x}Ge_x)\ S_5I$ ($x = 0.25, 0.5, 0.75$) crystals.

Composition	Temperature of the melt zone (K)	Temperature of the annealing zone (K)	Time of growth (hours)
$Ag_{6.25}P_{0.75}Ge_{0.25}S_5I$	1143	733	168
$Ag_{6.5}P_{0.5}Ge_{0.5}S_5I$	1183	763	168
$Ag_{6.75}P_{0.25}Ge_{0.75}S_5I$	1203	773	168

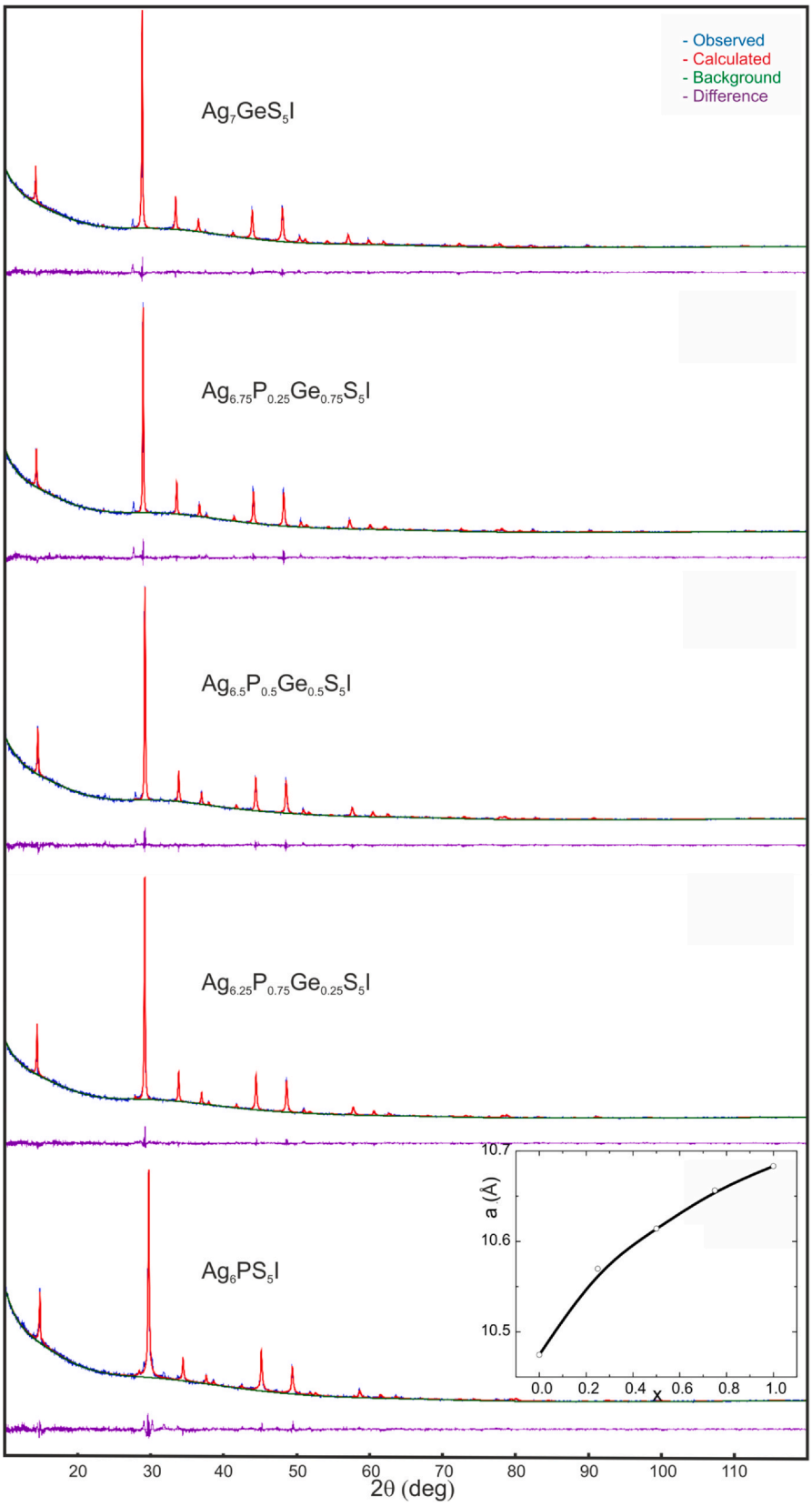

Fig. 1. Experimental and calculated diffractograms of $Ag_{6+x}(P_{1-x}Ge_x)S_5I$. The insert shows the compositional dependence of the parameter of the elementary cell for $Ag_{6+x}(P_{1-x}Ge_x)S_5I$.

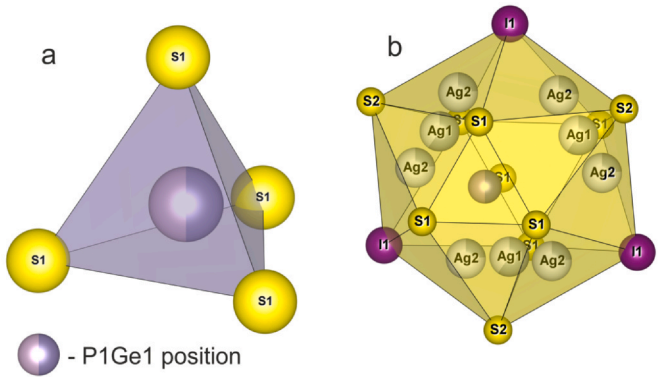

Fig. 2. [(PGe)S_4] tetrahedra (a) and [SS_9I_3] icosahedron (b) in the structure of $Ag_{6.5}P_{0.5}Ge_{0.5}S_5I$ solid solution.

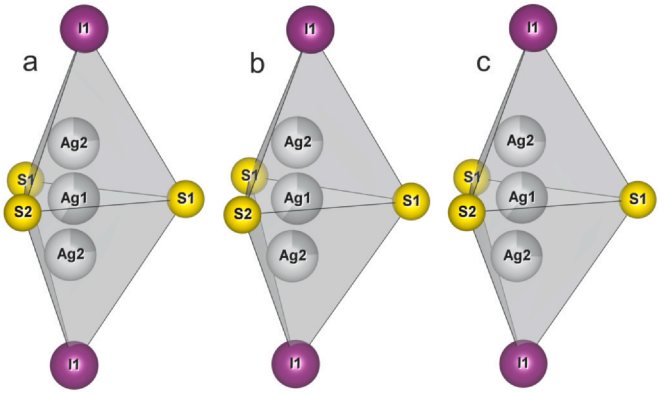

Fig. 3. [S_3I_2] doubled tetrahedra in the structure of $Ag_{6+x}(P_{1-x}Ge_x)S_5I$ solid solutions: (a) $Ag_{6.25}P_{0.75}Ge_{0.25}S_5I$, (b) $Ag_{6.5}P_{0.5}Ge_{0.5}S_5I$, (c) $Ag_{6.75}P_{0.25}Ge_{0.75}S_5I$.

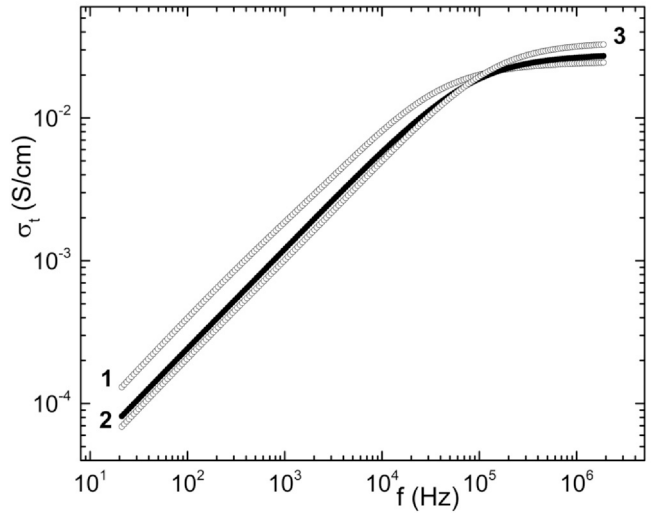

Fig. 4. Frequency dependences of total electrical conductivity for $Ag_{6+x}(P_{1-x}Ge_x)S_5I$ solid solutions at $T = 298$ K: (1) $Ag_{6.25}P_{0.75}Ge_{0.25}S_5I$, (2) $Ag_{6.5}P_{0.5}Ge_{0.5}S_5I$, (3) $Ag_{6.75}P_{0.25}Ge_{0.75}S_5I$.

3.2. Electrical conductivity

Fig. 4. shows the frequency dependences of the total electrical conductivity for $Ag_{6+x}(P_{1-x}Ge_x)S_5I$ solid solutions. The frequency dependences of the total electrical conductivity showed a growth of conductivity with increasing frequency for all compositions. For detailed studies of frequency dependences of electrical conductivity

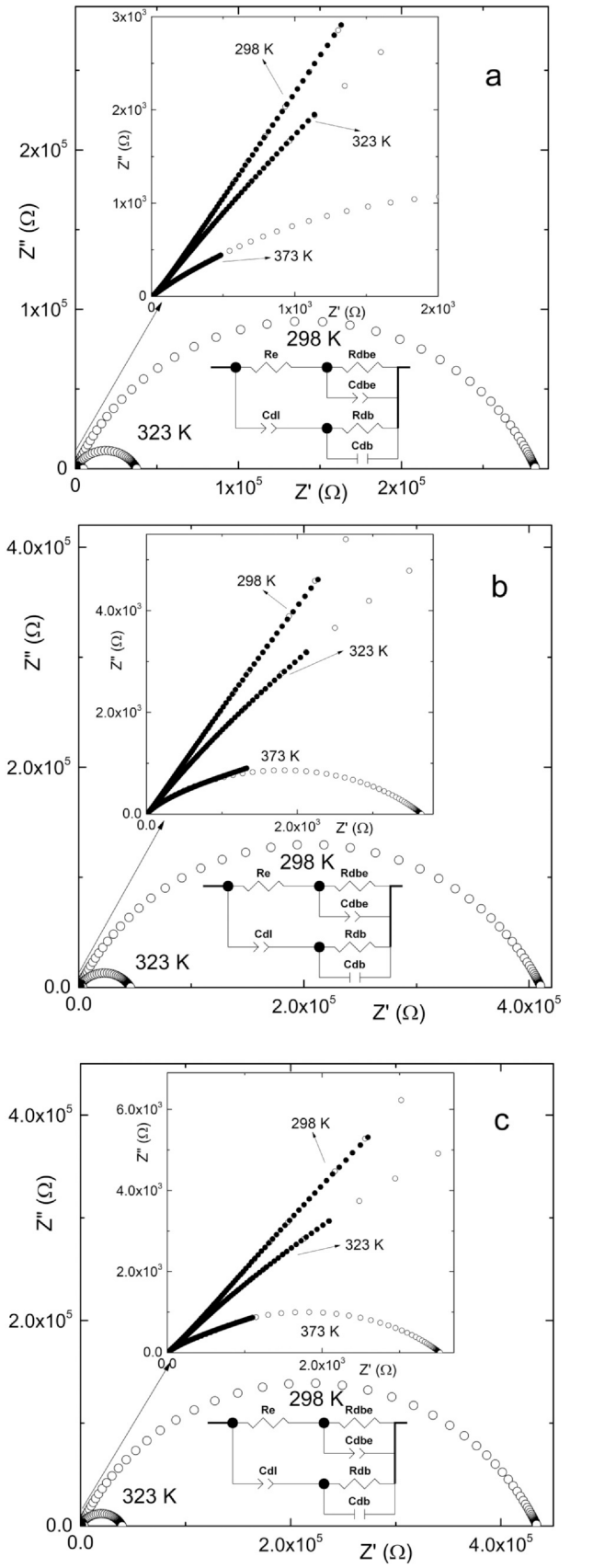

Fig. 5. EEC and Nyquist plots for $Ag_{6+x}(P_{1-x}Ge_x)S_5I$ solid solutions at different temperatures: (a) $Ag_{6.25}P_{0.75}Ge_{0.25}S_5I$, (b) $Ag_{6.5}P_{0.5}Ge_{0.5}S_5I$, (c) $Ag_{6.75}P_{0.25}Ge_{0.75}S_5I$. Experimental data correspond to the solid dots, calculated data correspond to the open dots.

and its separation into ionic and electronic components, a standard approach with the use of electrode equivalent circuits (EEC) and analysis of the Nyquist plots was used [31–33]. The parasitic inductance of the cell (~2×10^{-8} H) was taken into account during the analysis.

Single-crystal samples of $Ag_{6+x}(P_{1-x}Ge_x)S_5I$ ($x = 0.25, 0.5, 0.75$) solid solutions are characterized by a rather low value of electronic conductivity ($\sigma_{ion} > \sigma_{el}$), which led to the displacement of the low-frequency semicircle in the low-frequency region, which is the evidence of the influence of diffusion and relaxation processes. On the Z′-Z dependencies, two semicircles are observed for all solid solution compositions at a temperature of 298 K, and the high-frequency semicircle is very weakly expressed (Fig. 5), and when the temperature rises, they degenerate into one semicircle. For the description of Nyquist plots of all solid solutions, one EEC is chosen, which can be divided into two parts, describing the processes associated with ionic and electronic components of electrical conductivity, respectively.

Diffusion relaxation processes at the electrode/crystal boundary correspond to low-frequency semicircles on Nyquist plots, which is expressed by the included capacity of the double diffusion layer C_{dl} (Fig. 5). The prevailing influence of diffusion and relaxation ion processes, against the background of sufficiently low values of electronic and ionic components of electrical conductivity, leads to a fuzzy representation of high-frequency semicircles, which in turn are described by the processes of electrical conductivity on domain boundaries, which is represented on EEC by the serially connected resistance R_{db} (Fig. 7) with parallel-connected capacitance C_{db}. Thus, the ionic conductivity of $Ag_{6+x}(P_{1-x}Ge_x)S_5I$ ($x = 0.25, 0.5, 0.75$) solid solutions is determined by the resistance of domain boundaries R_{db}. Nature of domains in $Ag_{6+x}(P_{1-x}Ge_x)S_5I$ ($x = 0.25, 0.5, 0.75$) solid solutions, as in the case of Ag_6PS_5I and Ag_7GeS_5I, is possibly associated with the presence of a mosaic texture of a crystal. In this case, the domain boundaries represent a structural heterogeneity, which manifests itself in the disorientation of texture elements <1° [34].

Parallel to the elements responsible for the ionic processes, the EEC includes elements responsible for the electronic component of electrical conductivity, namely the electronic resistance R_e and the electronic resistance of the domain boundaries R_{dbe} with parallelly connected capacitance C_{dbe}, which contributes to the representation of both semicircles on Nyquist plots. Consequently, the electronic component of the electrical conductivity of $Ag_{6+x}(P_{1-x}Ge_x)S_5I$ ($x = 0.25, 0.5, 0.75$) solid solutions is determined by the sum of the resistance of the domain boundaries R_{dbe} and the resistance R_e.

EEC, which is shown in Fig. 5, well describes the temperature behavior of impedance of single crystals of solid solutions in the temperature interval 293–383 K, as well as ionic and electronic processes occurring in the materials under study. This is evidenced by the sequential degeneration of two semicircles into one observed at a temperature above 323 K, due to a significant increase in the ionic component of electrical conductivity.

The analysis of impedance spectra made it possible to investigate compositional (Fig. 6a) and temperature (Fig. 7) dependences of ionic and electronic components of electrical conductivity of single crystals of $Ag_{6+x}(P_{1-x}Ge_x)S_5I$ ($x = 0.25, 0.5, 0.75$) solid solutions.

It is established that the compositional dependence of the ionic component of electrical conductivity (Fig. 6a, curve 1) has a non-monotonous nonlinear character, which manifests itself in its sharp growth at $P^{+5} \rightarrow Ge^{+4}$ cationic substitution within the anionic sublattice, compared with initial ternary Ag_6PS_5I and Ag_7GeS_5I. Thus, the value of the ionic component of electrical conductivity is 1.79×10^{-3} S/cm for Ag_6PS_5I and 7.98×10^{-3} S/cm for Ag_7GeS_5I [19], whereas for $Ag_{6+x}(P_{1-x}Ge_x)S_5I$ ($x = 0.25, 0.5, 0.75$) solid solutions its value is in the range from 2.4×10^{-2} S/cm to 2.9×10^{-2} S/cm. Instead, the value of the electronic component of electrical conductivity (Fig. 6a, curve 2), which for Ag_6PS_5I is 1.64×10^{-6} S/cm at $P^{+5} \rightarrow Ge^{+4}$

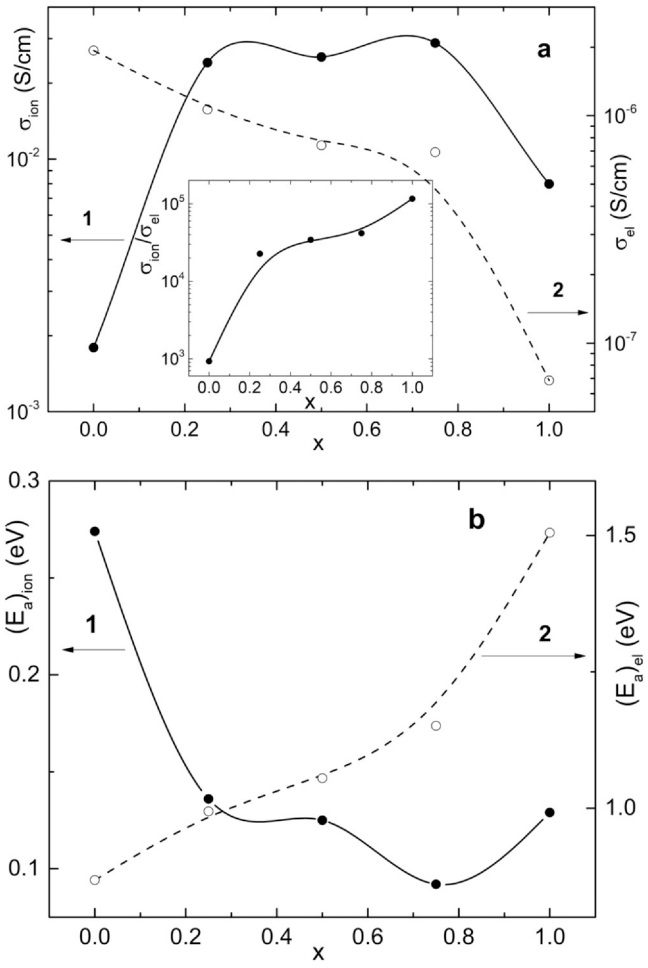

Fig. 6. Compositional dependences of ionic (1) and electronic (2) components of electrical conductivity (a) as well as the activation energies (b) of ionic (1) and electronic (2) components of electrical conductivity at $T = 298$ K for $Ag_{6+x}(P_{1-x}Ge_x)S_5I$ solid solutions. The insert shows the compositional dependence of the ratio of the conductivity components for $Ag_{6+x}(P_{1-x}Ge_x)\ S_5I$ solid solutions.

cationic substitution decreases without any features on the compositional dependence. On the insert to Fig. 6a the compositional dependence of the ratio of the ionic component of electrical conductivity to electronic one is shown. It is established that for $Ag_{6+x}(P_{1-x}Ge_x)\ S_5I$ ($x = 0.25, 0.5, 0.75$) solid solutions the ionic component is more than 10^4 times higher than the electronic one.

In Fig. 7 the temperature dependences of the ionic (curve 1) and electronic (curve 2) components of electrical conductivity in Arrhenius coordinates are shown. It is established that they have a linear character and are described by Arrhenius law, which indicates the thermoactivation mechanism of electrical conductivity. With their help, the activation energies of both ionic and electronic conductivity components were determined (Fig. 6b). The compositional dependence of the activation energy of ionic conductivity (Fig. 6b, curve 1) shows a nonlinear decrease in the activation energy in solid solutions, which for $Ag_{6.75}P_{0.25}Ge_{0.75}S_5I$ reaches a minimum (0.092 eV). In this case, the activation energy of electronic conductivity at $P^{+5} \rightarrow Ge^{+4}$ cationic substitution (Fig. 6b, curve 2) increases nonlinearly without any features.

3.3. Mechanism of ionic conductivity

Let us consider the mechanism of ion transport for $Ag_{6+x}(P_{1-x}Ge_x)S_5I$ ($x = 0.25, 0.5, 0.75$) solid solutions. Although Ag1 (24 g) is located in the plane of the triangle S1S2S1, the moving in the

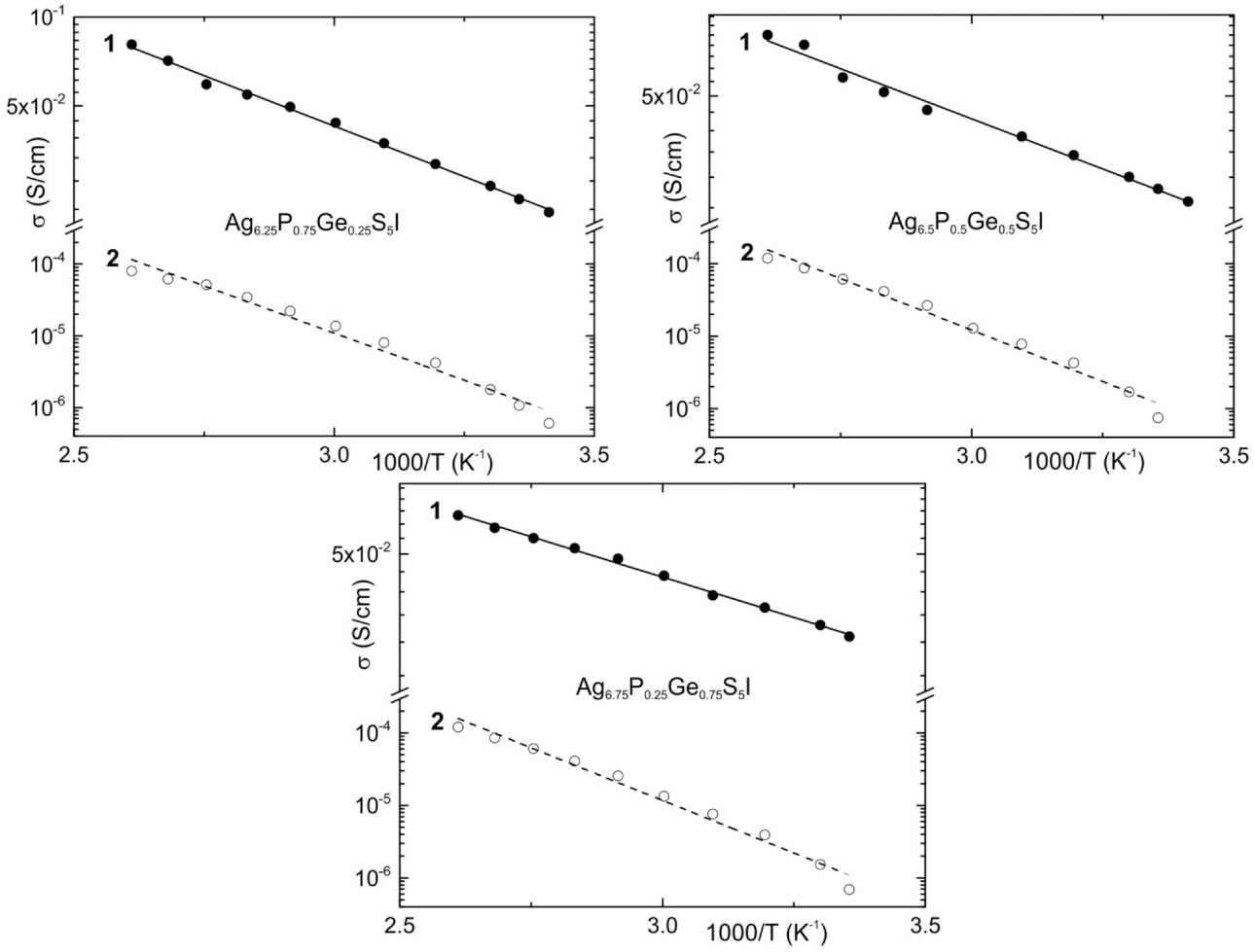

Fig. 7. Temperature dependences of ionic (1) and electronic (2) components of electrical conductivity for $Ag_{6+x}(P_{1-x}Ge_x)S_5I$ solid solutions.

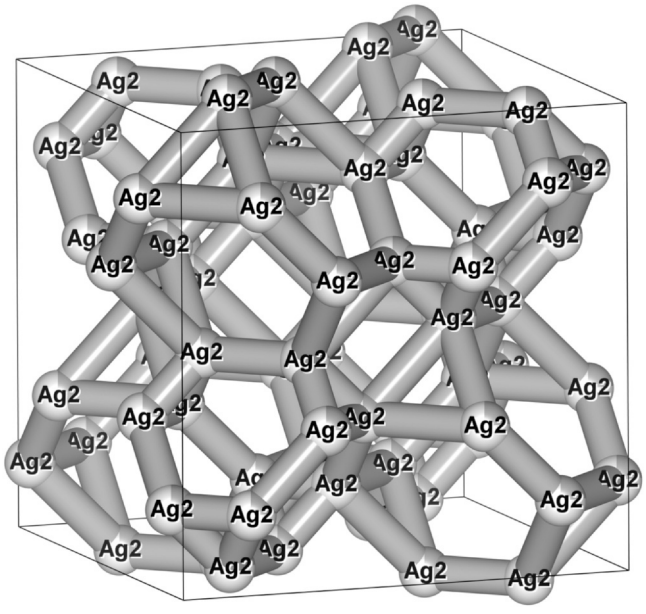

Fig. 8. The mechanism of ion transport for $Ag_{6.5}P_{0.5}Ge_{0.5}S_5I$ solid solution on the example of "grid" of mobile cations migration at Ag2 position.

structure is an atom in position Ag2 (48 h), which is shifted to the plane S1I1S2 and to the edge S2I. This is explained by the smaller values of SOF (site occupancy factor) Ag2 vs. Ag1, so the mechanism of ion transport can be considered as ion diffusion through "channels" Ag2–Ag2 (Fig. 8).

To estimate the efficiency of ion transport in $Ag_{6+x}(P_{1-x}Ge_x)\ S_5I$ solid solutions we use the SOF parameters and d_{max}, the first of which shows the disordering (mobility) of the position, and the second is limiting distance in the "grid" of mobile cations migration in Ag2 position.

As can be seen from Fig. 9a (curve 1), the maximal Ag2–Ag2 distance at cationic $P^{+5}\rightarrow Ge^{+4}$ substitution is characterized by a tendency to increase, but within small limits (2.88 – 3.09 Å). Instead, the compositional dependence of SOF for Ag2 (Fig. 9a, curve 2) is characterized by the presence of a minimum for the solid solution $Ag_{6.25}P_{0.75}Ge_{0.25}S_5I$ (0.228) in comparison with the initial quaternary Ag_6PS_5I and Ag_7GeS_5I, for which the SOF value is 0.239 and 0.273, respectively. Noteworthy is the fact that both d_{max} and SOF for $Ag_{6+x}(P_{1-x}Ge_x)S_5I$ ($x = 0.25, 0.5, 0.75$) solid solutions are smaller than for the Ag_7GeS_5I crystal, for which the value of the ionic component of conductivity is 7.98×10^{-3} S/cm [19], which should lead to better ion transport efficiency. However, for Ag_6PS_5I the ionic component (1.79×10^{-3} S/cm) of electrical conductivity is lower than for Ag_7GeS_5I, even if there are more favorable structural parameters. In addition, the nonlinear behavior of the compositional dependence of the ionic component of electrical conductivity (Fig. 6a, curve 1) and its activation energy (Fig. 6b, curve 1) can not be explained using parameters such as SOF for Ag2 and the maximal distance in the "grid" of mobile cations migration into position Ag2 (Fig. 9a).

Let us consider in this respect the $Ag_{6+x}(P_{1-x}Ge_x)\ S_5I$ ($x = 0.25, 0.5, 0.75$) solid solutions. Thus, for $Ag_{6.25}P_{0.75}Ge_{0.25}S_5I$ the smallest

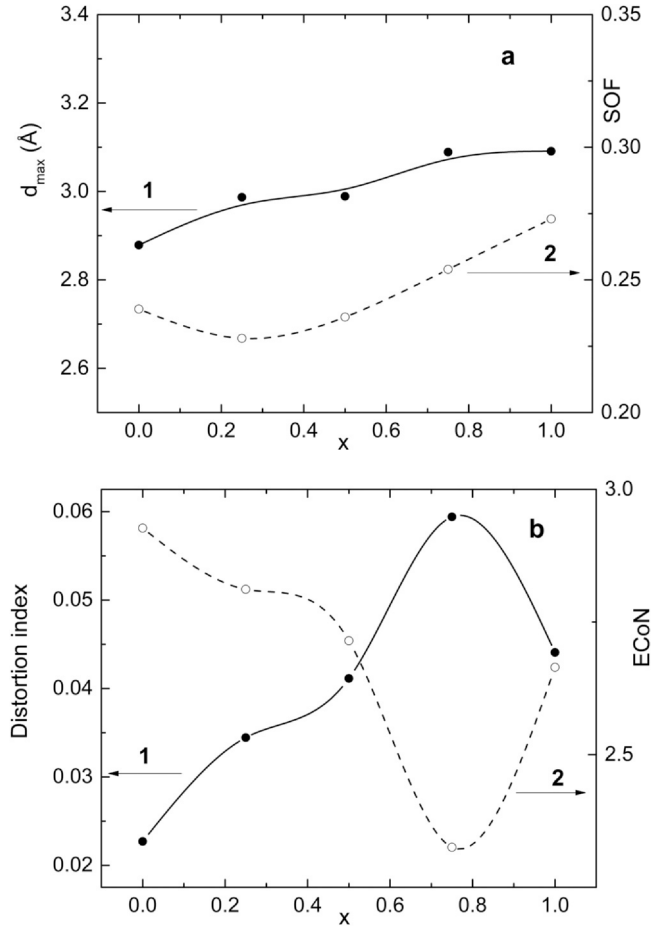

Fig. 9. Compositional dependences of d_{max} Ag2–Ag2 (a, curve 1) and SOF (a, curve 2) in the "grid" of mobile cations migration as well as the distortion index D (b, curve 1) and effective coordination number ECoN (b, curve 2).

values of d_{max} Ag2–Ag2 and SOF are observed on the compositional dependence of structural parameters (Fig. 9a). However, the highest value of the ionic component of electrical conductivity (Fig. 6a, curve 1) is observed not for $Ag_{6.25}P_{0.75}Ge_{0.25}S_5I$ solid solution (2.41×10^{-2} S/cm), but for $Ag_{6.75}$ $P_{0.25}Ge_{0.75}S_5I$ (2.88×10^{-2} S/cm), as well as for $Ag_{6.75}P_{0.25}Ge_{0.75}S_5I$ on the compositional dependence of the activation energy there is a minimum of 0.092 eV (Fig. 6b, curve 1). It becomes obvious that with all the importance of the influence of the above-described structural parameters on the efficiency of ion transport, its limiting factor may be somewhat different.

In this regard, let us consider the triangular pyramids Ag2S1S1S2 ($[AgS_3]$) (Fig. 10), which are a component of the doubled $[AgS_3I_2]$ tetrahedra (Fig. 3), which will allow estimating the displacement of the atom in position Ag2 relatively to the triangular plane S1S2 of $[S_3I_2]$ polyhedron.

To quantify the degree of displacement of Ag2 atom relatively to the triangular plane S1S1S2, we use the value of the distortion index D [30,35] and the effective coordination number ECoN [30, 36–39]. The distortion coefficient D is defined as the average value of the relative deviation of the Ag-S bond lengths in the above pyramid, whereas ECoN is defined as the sum of the contributions of each bond to the effective coordination number. The above parameters were calculated using VESTA 3 [30] program, and their compositional dependencies are shown in Fig. 9b.

It is established that the compositional behavior of the distortion index D (Fig. 9b, curve 1) and the effective coordination number ECoN (Fig. 9b, curve 2) for $Ag_{6+x}(P_{1-x}Ge_x)S_5I$ solid solutions is non-monotonous and nonlinear, which is manifested in the presence of the distortion index D maximum and, accordingly, the ECoN minimum observed for $Ag_{6.75}P_{0.25}Ge_{0.75}S_5I$. From this, it follows that for $Ag_{6+x}(P_{1-x}Ge_x)S_5I$ ($x = 0.25$, 0.5, 0.75) solid solutions, the displacement of the atom at the Ag2 position relative to the S1S2 triangular plane is greater than for Ag_6PS_5I, and for $Ag_{6.75}P_{0.25}Ge_{0.75}S_5I$, this displacement is greater than for both initial quaternary halogenchalcogenides, which certainly contributes to the Ag2 ion transport in the "grid" of mobile cation migration (Fig. 8).

We would analyze the nonlinear change of the ionic component of electrical conductivity (Fig. 6a, curve 1) using the distortion index D and the activation energy (Fig. 6b, curve 1) of ionic conductivity using ECoN. In the process of heterovalent cationic $P^{+5} \rightarrow Ge^{+4}$ substitution for $Ag_{6.25}P_{0.75}Ge_{0.25}S_5I$ solid solution there is a sharp increase in the ionic component of electrical conductivity (Fig. 6a, curve 1), which is associated with the growth of the distortion index D (Fig. 9b, curve 1) and SOF minimum (Fig. 9a, curve 2). With further increase in the number of Ge^{+4} cations, despite the rapid increase in the distortion index D, the ionic component of electrical conductivity increases gradually enough, which is associated with the gradual increase in SOF, and for $Ag_{6.75}P_{0.25}Ge_{0.75}S_5I$ solid solution, it reaches its maximum value, like the distortion index.

A similar compositional behavior is observed for the activation energy of the ionic component of electrical conductivity (Fig. 6b, curve 1), which almost completely depends on the change in the ECoN parameter (Fig. 9b, curve 2).

Thus, it can be concluded that in the presence of favorable structural parameters (small values of SOF and *d*max), which allow evaluating the efficiency of ion transport, no less important are the parameters that allow to determine the degree of displacement of

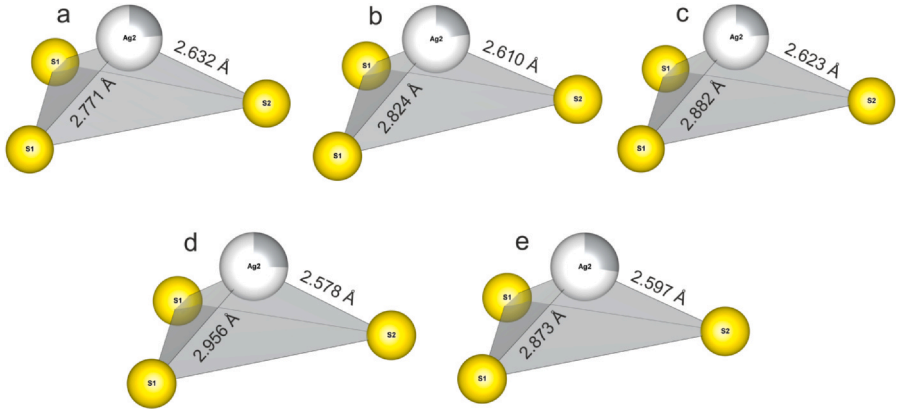

Fig. 10. $[AgS_3]$ triangular pyramid in the structure of $Ag_{6+x}(P_{1-x}Ge_x)S_5I$: (a) Ag_6PS_5I, (b) $Ag_{6.25}P_{0.75}Ge_{0.25}S_5I$, (c) $Ag_{6.5}P_{0.5}Ge_{0.5}S_5I$, (d) $Ag_{6.75}P_{0.25}Ge_{0.75}S_5I$, (e) Ag_7GeS_5I.

the mobile cation within the polyhedra (D, ECoN) and explain in detail the features of ion transport in the material under study.

4. Conclusions

Synthesis of $Ag_{6+x}(P_{1-x}Ge_x)S_5I$ ($x = 0.25, 0.5, 0.75$) compounds was carried out as well as the single crystals of dark gray color with metallic luster, 30–40 mm in length and 10–12 mm in diameter were grown from solution-melt using vertical crystallization method.

Using the full-profile analysis by the Rietveld method, we established that a continuous series of solid solutions is formed in Ag_6PS_5I – Ag_7GeS_5I system. The crystal structure of $Ag_{6+x}(P_{1-x}Ge_x)S_5I$ ($x = 0.25, 0.5, 0.75$) is calculated, as a result of which the basic structural parameters are determined. The main structural features caused by heterovalent cationic $P^{+5} \leftrightarrow Ge^{+4}$ substitution within an anionic sublattice are established and discussed as well as their influence on the cationic sublattice on the example of structure-forming polyhedra is shown.

Total electrical conductivity is measured by impedance spectroscopy using gold contacts in the frequency range from 10 Hz to 2 MHz and temperature interval 293–383 K on single-crystal samples of $Ag_{6+x}(P_{1-xGe\ x})\ S_5I$ ($x = 0.25, 0.5, 0.75$) solid solutions. Based on the frequency dependences of the total electrical conductivity, Nyquist plots were constructed, which were further analyzed using electrode equivalent circuits. Using this approach, the total electrical conductivity was divided into ionic and electronic components, which allowed to build their compositional dependence and determine the σ_{ion}/σ_{el} ratio. It is established that the temperature dependences of the ionic and electronic components of electrical conductivity are linear and are described by Arrhenius law, which indicates the thermoactivation mechanism of electrical conductivity. According to the results of temperature studies, activation energies of both ionic and electronic component of electrical conductivity were determined.

The peculiarities of ion transport mechanism in $Ag_{6+x}(P_{1-x}Ge_x)S_5I$ ($x = 0.25, 0.5, 0.75$) solid solutions are explained on the basis of analyzing the features of crystal structure, compositional behavior of the ionic component electrical conductivity and its activation energy.

Declaration of Competing Interest

The authors declare that they have no known competing financial interests or personal relationships that could have appeared to influence the work reported in this paper.

References

[1] W.F. Kuhs, R. Nitsche, K. Scheunemann, The argyrodites - a new family of tetrahedrally close-packed structures, Mat. Res. Bull. 14 (2) (1979) 241–248, https://doi.org/10.1016/0025-5408(79)90125-9

[2] T. Nilges, A. Pfitzner, A structural differentiation of quaternary copper argyrodites: structure – property relations of high temperature ion conductors, Z. Krist. 220 (2005) 281–294, https://doi.org/10.1524/zkri.220.2.281.59142

[3] H.-J. Deiseroth, S.-T. Kong, H. Eckert, J. Vannahme, C. Reiner, T. Zaiss, M. Schlosser, Li_6PS_5X: a class of crystalline Li-rich solids with an unusually high Li^+ mobility, Angew. Chem. Int. Ed. Engl. 47 (4) (2008) 755–758, https://doi.org/10.1002/anie.200703900

[4] H.-J. Deiseroth, J. Maier, K. Weichert, V. Nickel, S.-T. Kong, C. Reiner, Li_7PS_6 and Li_6PS_5X (X: Cl, Br, I): possible three-dimensional diffusion pathways for lithium ions and temperature dependence of the ionic conductivity by impedance measurements, Z. Anorg. Allg. Chem. 637 (2011) 1287–1294, https://doi.org/10.1002/zaac.201100158

[5] H.M. Chen, C. Maohua, S. Adams, Stability and ionic mobility in argyrodite-related lithium-ion solid electrolytes, Phys. Chem. Chem. Phys. 17 (25) (2015) 16494–16506, https://doi.org/10.1039/C5CP01841B

[6] I.P. Studenyak, V.O. Stefanovich, M. Kranjcec, D.I. Desnica, Yu.M. Azhnyuk, Gy.Sh. Kovacs, V.V. Panko, Raman scattering studies of Cu_6PS_5Hal (Hal=Cl,Br,I) fast-ion conductors, Solid State Ion. 95 (1997) 221–225, https://doi.org/10.1016/S0167-2738(96)00477-8

[7] R.B. Beeken, J.J. Garbe, J.M. Gillis, N.R. Petersen, B.W. Podoll, M.R. Stoneman, Electrical conductivities of the Ag_6PS_5X and the Cu_6PSe_5X (X=Br, I) argyrodites, J. Phys. Chem. Solids 66 (5) (2005) 882–886, https://doi.org/10.1016/j.jpcs.2004.10.010

[8] R.B. Beeken, J.J. Garbe, N.R. Petersen, M.R. Stoneman, Electrical properties of the Ag_6PSe_5X (X=Cl, Br, I) argyrodites, J. Phys. Chem. Solids 65 (5) (2004) 1011–1014, https://doi.org/10.1016/j.jpcs.2003.10.060

[9] E. Gaudin, V. Petricek, F. Boucher, F. Taulelle, M. Evain, Structures and phase transitions of the A_7PSe_6 (A = Ag, Cu) argyrodite-type ionic conductors. III. alpha-Cu_7PSe_6, Acta Crystallogr. B 56 (2000) 972–979, https://doi.org/10.1107/s0108768100010260

[10] A.I. Pogodin, M.J. Filep, T.O. Malakhovska, M.Yu Sabov, V.I. Sidey, O.P. Kokhan, I.P. Studenyak, The copper argyrodites Cu7-PS6-Br: Crystal growth, structures and ionic conductivity, Solid State Ion. 341 (2019) 115023, https://doi.org/10.1016/j.ssi.2019.115023

[11] P. Adeli, J.D. Bazak, K.H. Park, I. Kochetkov, A. Huq, G.R. Goward, L.F. Nazar, Boosting solid-state diffusivity and conductivity in lithium superionic argyrodites by halide substitution, Angew. Chem. Int. Ed. 58 (2019) 8681–8686, https://doi.org/10.1002/anie.201814222

[12] Y. Tomm, S. Schorr, S. Fiechter, Crystal growth of argyrodite-type phases $Cu_{8-x}GeS_6$-xI_x and $Cu_{8-x}GeSe_{6-x}I_x$ (0≤x≤0.8), J. Cryst. Growth 310 (2008) 2215–2221, https://doi.org/10.1016/j.jcrysgro.2007.11.184

[13] I.P. Studenyak, V.Yu Izai, V.I. Studenyak, A.I. Pogodin, M.Y. Filep, O.P. Kokhan, B. Grančič, P. Kúš, Interrelations between structural and optical properties of $(Cu_{1-x}Ag_x)_7GeS_5I$ mixed crystals, Ukr. J. Phys. Opt. 19 (No 4) (2018) 237–243, https://doi.org/10.3116/16091833/19/4/237/2018

[14] I.P. Studenyak, A.I. Pogodin, V.I. Studenyak, V.Yu Izai, M.J. Filep, O.P. Kokhan, M. Kranjčec, P. Kúš, Electrical properties of copper- and silver-containing superionic $(Cu_{1-x}Ag_x)_7SiS_5I$ mixed crystals with argyrodite structure, Solid State Ion. 345 (2020) 115183, https://doi.org/10.1016/j.ssi.2019.115183

[15] I. Semkiv, H. Ilchuk, M. Pawlowski, V. Kusnezh, Ag_8SnSe_6 argyrodite synthesis and optical properties, Opto-Electron. Rev. 25 (2017) 37–40, https://doi.org/10.1016/j.opelre.2017.04.002

[16] R. Chen, P. Qiu, B. Jiang, P. Hu, Y. Zhang, J. Yang, D. Ren, X. Shia, L. Chen, Significantly optimized thermoelectric properties in high-symmetry cubic Cu_7PSe_6 compounds via entropy engineering, J. Mater. Chem. A. 6 (2018) 6493–6502, https://doi.org/10.1039/C8TA00631H

[17] F. Reissig, B. Heep, M. Panthöfer, M. Wood, S. Anand, G.J. Snyder, W. Tremel, Effect of anion substitution on the structural and transport properties of argyrodites $Cu_7PSe_{6-x}S_x$, Dalton Trans. 48 (2019) 15822–15829, https://doi.org/10.1039/C9DT03247A

[18] X. Shen, C.-C. Yang, Y. Liu, G. Wang, H. Tan, Y.-H. Tung, G. Wang, X. Lu, J. He, X. Zhou, High-temperature structural and thermoelectric study of argyrodite Ag_8GeSe_6, ACS Appl. Mater. Interfaces 11 (2) (2019) 2168–2176, https://doi.org/10.1021/acsami.8b19819

[19] I.P. Studenyak, A.I. Pogodin, V.I. Studenyak, M.J. Filep, O.P. Kokhan, P. Kús, Y.M. Azhniuk, D.R.T. Zahn, Structure, electrical conductivity, and Raman spectra of (Cu1–Ag)7GeS5I and (Cu1–Ag)7GeSe5I mixed crystals, Mater. Res. Bull. 135 (2021) 111116, https://doi.org/10.1016/j.materresbull.2020.111116

[20] I.P. Studenyak, A.I. Pogodin, O.P. Kokhan, V. Kavaliukė, T. Šalkus, A. Kežionis, A.F. Orliukas, Crystal growth, structural and electrical properties of $(Cu_{1-x}Ag_x)_7GeS_5I$ superionic solid solutions, Solid State Ion. 329 (2019) 119–123, https://doi.org/10.1016/j.ssi.2018.11.020

[21] Z. Zhang, Y. Sun, X. Duan, L. Peng, H. Jia, Y. Zhang, B. Shan, J. Xie, Design and synthesis of room temperature stable Li-argyrodite superionic conductors via cation doping, J. Mater. Chem. A. 7 (2019) 2717–2722, https://doi.org/10.1039/C8TA10790D

[22] MA. Kraft, S. Ohno, T. Zinkevich, R. Koerver, S.P. Culver, T. Fuchs, A. Senyshyn, S. Indris, B.J. Morgan, W.G. Zeier, Inducing high ionic conductivity in the lithium superionic argyrodites $Li_{6+x}P_{1-x}Ge_xS_5I$ for all-solid-state batteries, J. Am. Chem. Soc. 140 (47) (2018) 16330–16339, https://doi.org/10.1021/jacs.8b10282

[23] S. Ohno, B. Helm, T. Fuchs, G. Dewald, M.A. Kraft, S.P. Culver, A. Senyshyn, W.G. Zeier, Further evidence for energy landscape flattening in the superionic argyrodites $Li_{6+x}P_{1-x}M_xS_5I$ (M = Si, Ge, Sn), Chem. Mater. 31 (13) (2019) 4936–4944, https://doi.org/10.1021/acs.chemmater.9b01857

[24] N. Minafra, S.P. Culver, T. Krauskopf, A. Senyshyn, W.G. Zeier, Effect of Si substitution on the structural and transport properties of superionic Li-argyrodites, J. Mater. Chem. A. 6 (2018) 645–651, https://doi.org/10.1039/C7TA08581H

[25] M. Laqibi, B. Cros, S. Peytavin, M. Ribes, New silver superionic conductors Ag_7XY_5Z (X = Si, Ge, Sn; Y = S, Se; Z = Cl, Br, I)-synthesis and electrical studies, Solid State Ion. 23 (No 1–2) (1987) 21–26, https://doi.org/10.1016/0167-2738(87)90077-4

[26] H.M. Rietveld, A profile refinement method for nuclear and magnetic structures, J. Appl. Crystallogr. 2 (2) (1969) 65–71, https://doi.org/10.1107/S0021889869006558

[27] L.B. McCusker, R.B. Von Dreele, D.E. Cox, D. Louër, P. Scardi, Rietveld refinement guidelines, J. Appl. Crystallogr. 32 (1) (1999) 36–50, https://doi.org/10.1107/S0021889898009856

[28] A. Altomare, M.C. Burla, M. Camalli, B. Carrozzini, G.L. Cascarano, C. Giacovazzo, A. Guagliardi, A.G.G. Moliterni, G. Polidori, R. Rizzi, EXPO: a program for full powder pattern decomposition and crystal structure solution, J. Appl. Crystallogr. 32 (2) (1999) 339–340, https://doi.org/10.1107/S0021889898007729

[29] A. Altomare, C. Cuocci, C. Giacovazzo, A. Moliterni, R. Rizzi, N. Corriero, A. Falcicchio, EXPO2013: a kit of tools for phasing crystal structures from powder data, J. Appl. Crystallogr. 46 (4) (2013) 1231–1235, https://doi.org/10.1107/S0021889813013113

[30] K. Momma, F. Izumi, VESTA 3 for three-dimen-sional visualization of crystal, volumetric and morphology data, J. Appl. Crystallogr. 44 (2011) 1272–1276, https://doi.org/10.1107/S0021889811038970
[31] M.E. Orazem, B. Tribollet, Electrochemical Impedance Spectroscopy, John Wiley & Sons, New Jersey, 2008, https://doi.org/10.1002/9780470381588
[32] A.K. Ivanov-Schitz, I.V. Murin, Solid State Ionics, Univ. Press, St. Petersburg, 2000.
[33] R.A. Huggins, Simple method to determine electronic and ionic components of the conductivity in mixed conductors a review, Ionics 8 (3) (2002) 300–313, https://doi.org/10.1007/BF02376083
[34] A.R. West, Solid State Chemistry and Its Applications, 2nd ed., John Wiley & Sons, Ltd, 2014.
[35] W.H. Baur, The geometry of polyhedral distortions. predictive relationships for the phosphate group, Acta Crystallogr. Sect. B: Struct. Sci. 30 (1974) 1195–1215, https://doi.org/10.1107/S0567740874004560
[36] K. Robinson, G.V. Gibbs, P.H. Ribbe, Quadratic elongation: a quantitative measure of distortion in coordination polyhedral, Science 172 (3983) (1971) 567–570, https://doi.org/10.1126/science.172.3983.567
[37] R. Hoppe, Effective coordination numbers (ECoN) and mean fictive ionic radii (MEFIR), Z. Krist. 150 (1–4) (1979) 23–52, https://doi.org/10.1524/zkri.1979.150.14.23
[38] R. Hoppe, S. Voigt, H. Glaum, J. Kissel, H.P. Müller, K. Bernet, A new route to charge distributions in ionic solids, J. Less-Common Met. 156 (1–2) (1989) 105–122, https://doi.org/10.1016/0022-5088(89)90411-6
[39] C. Giacovazzo, H.L. Monaco, G. Artioli, D. Viterbo, M. Milanesio, G. Gilli, P. Gilli, G. Zanotti, G. Ferraris, M. Catti, Fundamentals of Crystallography, 3rd ed., Oxford University Press, Oxford, 2011, https://doi.org/10.1093/acprof:oso/9780199573653.001.0001